NASA/TM—2018-219905

Fractographic Analysis of 60-Nitinol Bearing Races

Malcolm K. Stanford
Glenn Research Center, Cleveland, Ohio

August 2018

NASA STI Program . . . in Profile

Since its founding, NASA has been dedicated to the advancement of aeronautics and space science. The NASA Scientific and Technical Information (STI) Program plays a key part in helping NASA maintain this important role.

The NASA STI Program operates under the auspices of the Agency Chief Information Officer. It collects, organizes, provides for archiving, and disseminates NASA's STI. The NASA STI Program provides access to the NASA Technical Report Server—Registered (NTRS Reg) and NASA Technical Report Server—Public (NTRS) thus providing one of the largest collections of aeronautical and space science STI in the world. Results are published in both non-NASA channels and by NASA in the NASA STI Report Series, which includes the following report types:

- TECHNICAL PUBLICATION. Reports of completed research or a major significant phase of research that present the results of NASA programs and include extensive data or theoretical analysis. Includes compilations of significant scientific and technical data and information deemed to be of continuing reference value. NASA counter-part of peer-reviewed formal professional papers, but has less stringent limitations on manuscript length and extent of graphic presentations.

- TECHNICAL MEMORANDUM. Scientific and technical findings that are preliminary or of specialized interest, e.g., "quick-release" reports, working papers, and bibliographies that contain minimal annotation. Does not contain extensive analysis.

- CONTRACTOR REPORT. Scientific and technical findings by NASA-sponsored contractors and grantees.

- CONFERENCE PUBLICATION. Collected papers from scientific and technical conferences, symposia, seminars, or other meetings sponsored or co-sponsored by NASA.

- SPECIAL PUBLICATION. Scientific, technical, or historical information from NASA programs, projects, and missions, often concerned with subjects having substantial public interest.

- TECHNICAL TRANSLATION. English-language translations of foreign scientific and technical material pertinent to NASA's mission.

For more information about the NASA STI program, see the following:

- Access the NASA STI program home page at http://www.sti.nasa.gov

- E-mail your question to help@sti.nasa.gov

- Fax your question to the NASA STI Information Desk at 757-864-6500

- Telephone the NASA STI Information Desk at 757-864-9658

- Write to:
  NASA STI Program
  Mail Stop 148
  NASA Langley Research Center
  Hampton, VA 23681-2199

NASA/TM—2018-219905

Fractographic Analysis of 60-Nitinol Bearing Races

Malcolm K. Stanford
Glenn Research Center, Cleveland, Ohio

National Aeronautics and
Space Administration

Glenn Research Center
Cleveland, Ohio 44135

August 2018

Acknowledgments

I am very grateful for the technical assistance I received during the course of this study from Joy A. Buehler, Terry R. McCue, and Dr. Richard B. Rogers. The enlightening technical discussions with Drs. Christopher DellaCorte and Rogers are also greatly appreciated. This work was funded by the Transformative Tools and Technologies (TTT) Project under NASA's Aeronautics Research Mission Directorate.

This report is a formal draft or working paper, intended to solicit comments and ideas from a technical peer group.

This work was sponsored by the Transformative Aeronautics Concepts Program.

Level of Review: This material has been technically reviewed by technical management.

Available from

NASA STI Program
Mail Stop 148
NASA Langley Research Center
Hampton, VA 23681-2199

National Technical Information Service
5285 Port Royal Road
Springfield, VA 22161
703-605-6000

This report is available in electronic form at http://www.sti.nasa.gov/ and http://ntrs.nasa.gov/

Fractographic Analysis of 60-Nitinol Bearing Races

Malcolm K. Stanford
National Aeronautics and Space Administration
Glenn Research Center
Cleveland, Ohio 44135

Abstract

Fracture surfaces on a failed bearing race made from 60-Nitinol (60 wt% Ni – 40 wt% Ti) were analyzed. The bearing had experienced excessive localized heat due to an issue during machining that may have resulted in dimensional distortion. However, the classical fracture features that were identified by scanning electron microscopy and the fracture origins coincided with high concentrations of TiC-based contamination. Lessons learned for processing and quality control are discussed. An attempt to use x-ray diffraction to directly measure residual stresses imparted from the required heat treatment is also discussed.

Introduction

60-Nitinol (60 wt% Ni – 40 wt% Ti) is a corrosion-resistant, highly-elastic, hardenable intermetallic material that is being developed by the National Aeronautics and Space Administration (NASA) for aerospace components (Refs. 1 to 3). Potential applications include gears and bearings that must be tolerant to damage and durable for long-duration exploration missions in corrosive environments.

Fractures were observed in some early prototype 60-Nitinol bearings after testing. These fractures originated on the inner diameter of the outer race and propagated outward radially. Some of the fractures appeared to propagate into the surface for only a short distance, but some went completely through the bearing races. One such bearing was disassembled, as shown in Figure 1. The manufacturing and processing history for this bearing was reviewed and a few possible causal factors for the fractures were considered (Ref. 4). It was thought that localized heating due to nonuniform contact with a grinding wheel during a machining operation led to warping of the bearing race. 60-Nitinol has also been found to warp due to the high levels of residual stress that are imparted to the material during its heat treatment process (Ref. 5). As the outer layers of material are removed, a part can warp as the residual stresses attempt to maintain equilibrium. Whatever caused the warping, the race was thought to have become dislodged from the machining fixture during the grinding process. This would have led to uneven grinding of the inner diameter later in the machining process. It was also thought that the bearing blank could have started out undersized such that there was not enough material to grind the bearing to its designed dimensions. In either case, the resulting out-of-round condition of the bearing was thought to have led to failure by fatigue, due to the cyclic loading of the asymmetrical part. The purpose of this study was to examine the microstructure of the failed bearing to better understand factors that could have influenced these fractures.

Procedures

Sections of the fractured bearing were cleaned ultrasonically in ethanol and then examined by low magnification optical microscopy and by scanning electron microscopy (SEM). By identifying the classical features found on a fracture surface, as shown schematically in Figure 2, the location of the fracture origin was determined. Further investigation enabled a determination of what initiated the fracture. After examination of the fracture surface, the region near one fracture origin was sectioned perpendicular to the fracture surface and prepared so the bulk material could be examined metallographically. The chemical composition of the bulk material was analyzed by inductively-coupled plasma atomic emission spectroscopy (ICP-AES). Chemical composition of selected features on the fracture surface and along the metallographic cross section were analyzed by energy-dispersive x-ray spectroscopy (EDS).

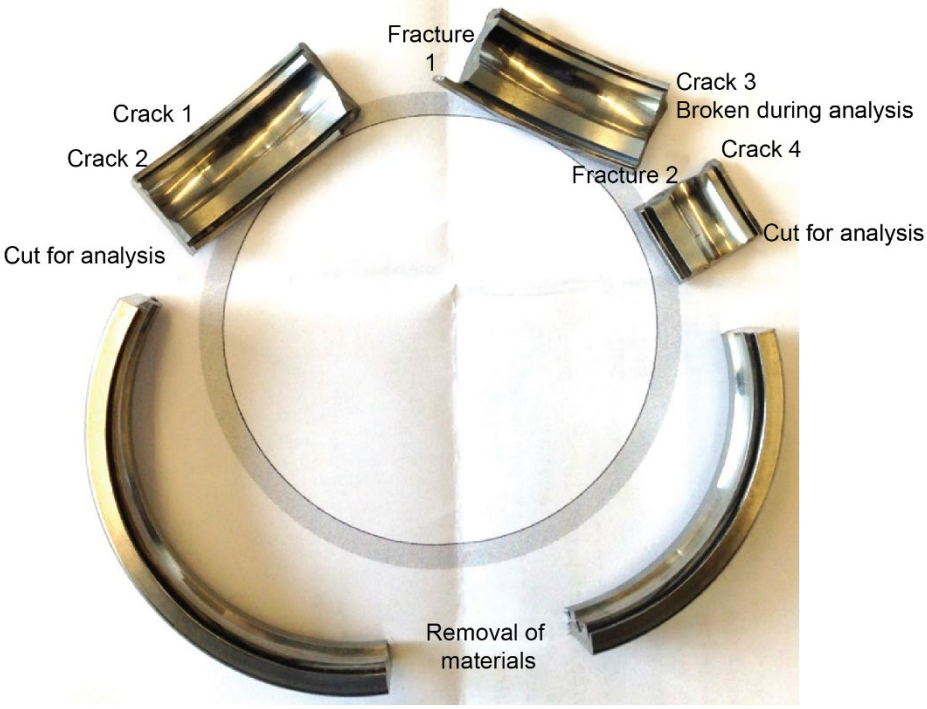

Figure 1.—Failed bearing sections with fracture surfaces for futher analysis labeled 1 and 2. In addition to the fractures, the bearing has been sectioned in a few locations to aid disassembly while preserving the fracture surfaces.

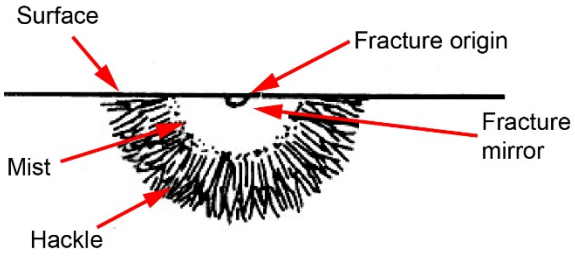

Figure 2.—Schematic representing the features of a brittle fracture initiating at a surface flaw (Ref. 6). Copyright 1992 from *Modern Ceramic Engineering: Properties, Processing, and Use in Design* by David W. Richerson. Reproduced by permission of Taylor and Francis Group, LLC, a division of Informa plc.

The crystal structure of the bearing was analyzed by x-ray diffraction (Ref. 7). This technique used a coherent source of x-rays with a wavelength that is the same order of magnitude as the lattice spacing of the sample. The x-rays interacted with the crystalline phases within the material through a range of impact angles, some causing destructive interference and some causing constructive interference, as illustrated schematically in Figure 3. The interference of the reflected x-rays is described by Bragg's law:

$$\sin\theta = \frac{\lambda}{2d_{hkl}}$$

where the impact angle θ is half the angle between the diffracted beam angle and the original beam angle, λ is the x-ray wavelength, and d_{hkl} is the lattice spacing. Since the x-ray wavelength and impact angles are

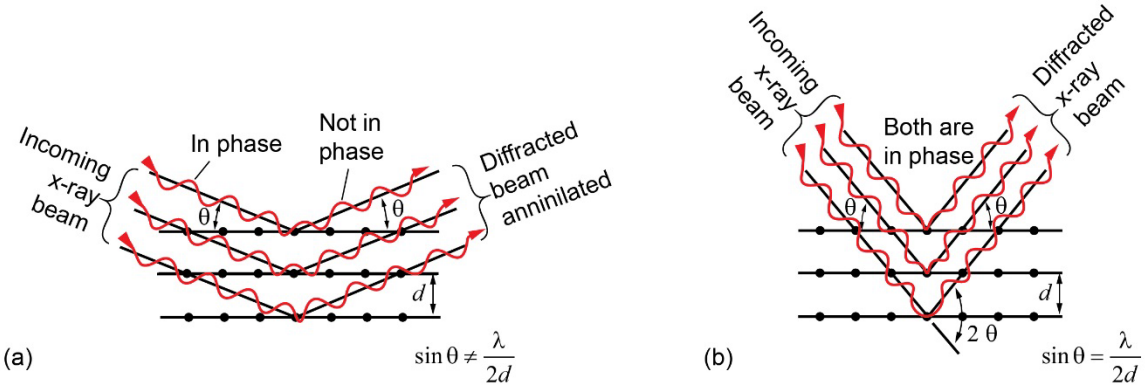

Figure 3.—Schematic representation of (a) destructive and (b) constructive interference between x-rays and the crystal structure of a sample during x-ray diffraction analysis (Ref. 7). Constructive interference occurs at angles that satisfy Bragg's law. The resultant diffraction pattern indicates exact atomic compositions with specific crystallographic structures. From Askeland/Phule. The Science and Engineering of Materials, 5E. © 2006 Cengage Learning, a part of Cengage, Inc. Reproduced by permission. www.cengage.com/permissions.

known, the lattice spacing can be determined. The lattice spacings were then compared to a database of known materials with precisely measured lattice spacings for identification of the phases present in the sample material.

To measure residual stresses created within typical 60-Nitinol bearings, two bearing blanks were procured. A bearing blank is a right circular cylinder that has been sectioned and machined by wire electric discharge machining to a size slightly greater than the designed dimensions so the part can be ground to its final dimensions. Both bearing blanks were machined from the same ingot of material. One of these bearing blanks was left in the condition rendered by hot isostatic pressing, which is essentially an annealed condition. In this case, the entire ingot of material was cooled slowly from approximately 980 °C, minimizing any residual stresses. The other bearing blank was heat treated at 1,000 °C for 2 hr and then water quenched. This heat treatment is used to harden 60-Nitinol but is thought to also impart residual stresses. X-ray diffractometers using Co Kα and Cu Kα radiation were used in an attempt to identify the spectral peaks associated with the known phases of 60-Nitinol, which include NiTi, Ni_3Ti, Ni_4Ti_3 and the metastable phase Ni_3Ti_2 (Refs. 8 and 9). The lattice spacings for the sample materials were to be compared to the known lattice spacings for 60-Nitinol to determine the effects of residual stress on 60-Nitinol.

Results and Discussion

Fractography

Figure 4 shows a macroscopic view of a fractured bearing surface with hackle (also known as "river patterns") indicating the location of the fracture initiation site. The inset shows the fracture initiation site at higher magnification. This fracture surface is from the fracture labeled "Fracture 1" in Figure 1. The mating half of the fracture surface shown in Figure 4 is shown in Figure 5, where the topography of the fracture surface can be observed with better resolution. Using backscattered electron imaging, as shown in Figure 6, the chemical difference between the bulk material and what is clearly an inclusion can be observed. Figure 7 shows EDS analysis of this inclusion, which indicates that it is composed of titanium, carbon and possibly nitrogen. A nitrogen peak appeared in the surrounding bulk material as well so, based on this analysis, it is not possible to determine if the inclusion is a compound of Ti, C and N (TiCN) or just Ti and C (TiC). There is also an interference between Ti and N peaks at roughly 0.5 keV that makes detection of N difficult in this material.

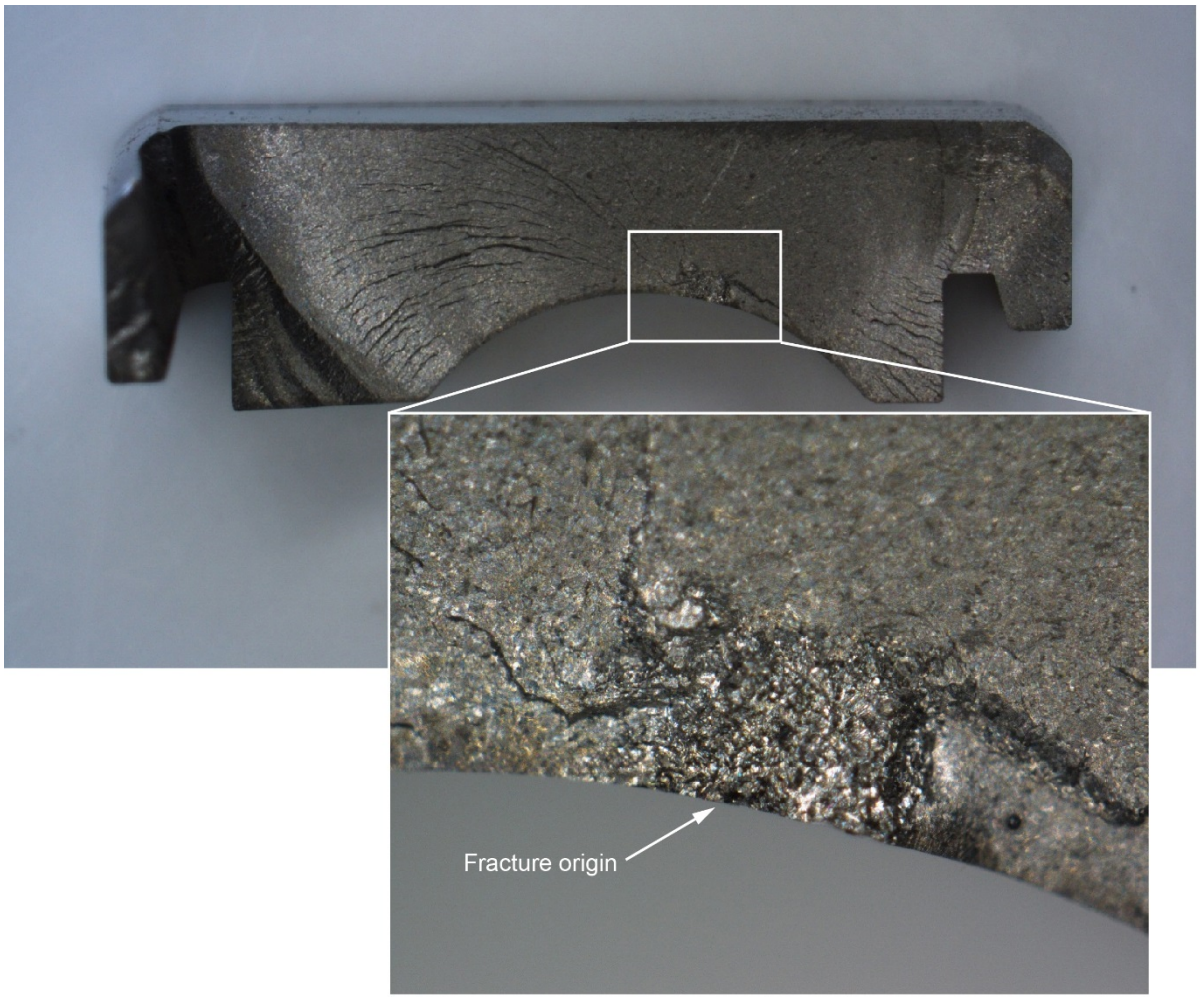

Figure 4.—Macroscopic image of fracture surface 1 with inset showing the fracture initiation site. Though the location of the fracture origin is easily identified by following the classical features identified in Figure 2, more depth of field is needed to further investigate the fracture origin.

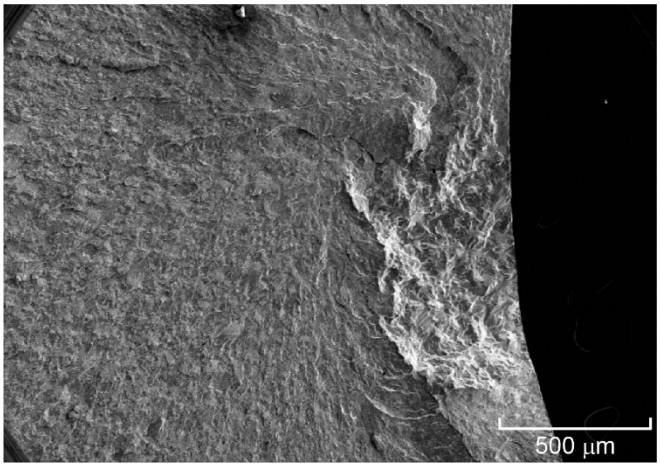

Figure 5.—SEM micrograph of the mating fracture surface to that shown in Figure 4. The topography of the surface is more clearly resolved with electron microscopy than with optical microscopy.

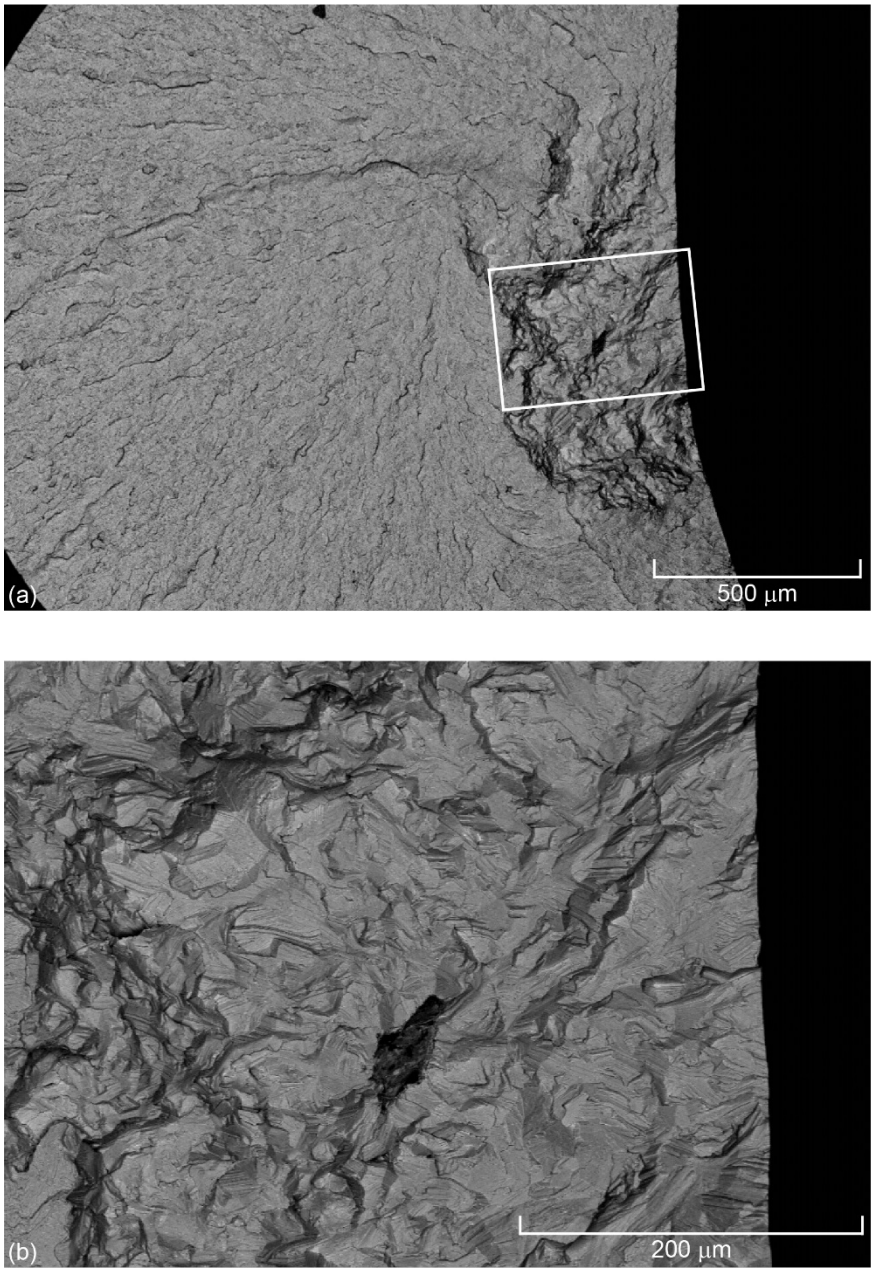

Figure 6.—Backscattered electron image SEM micrographs of the fracture initiation site from Figure 4 at (a) low and (b) high magnification, showing a large (approximately 75 μm in length) inclusion.

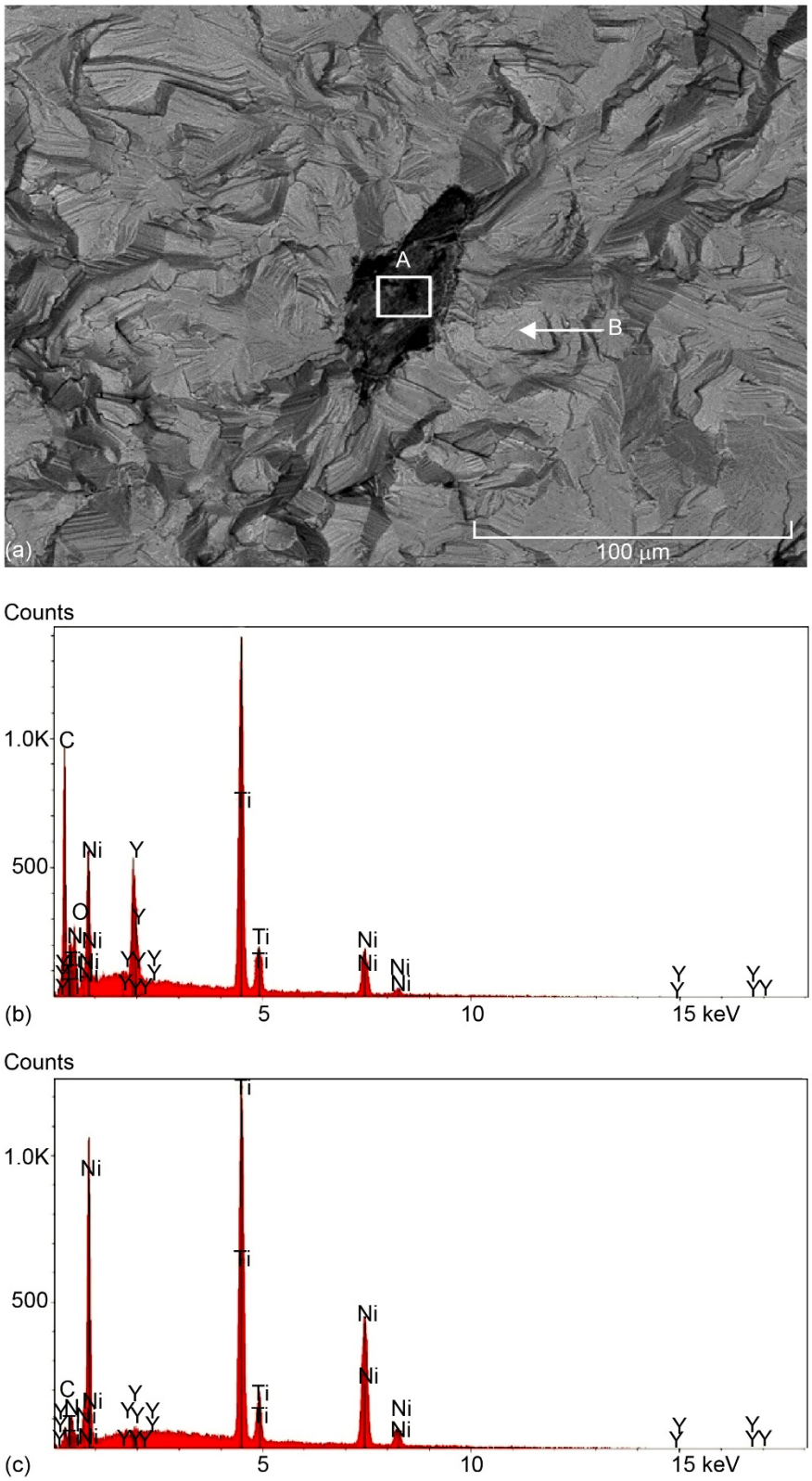

Figure 7.—SEM micrograph of the inclusion noted in Figure 6(b) and EDS spectra (b) at area A and (c) at point B indicating that the inclusion is composed of Ti, C and N within NiTi.

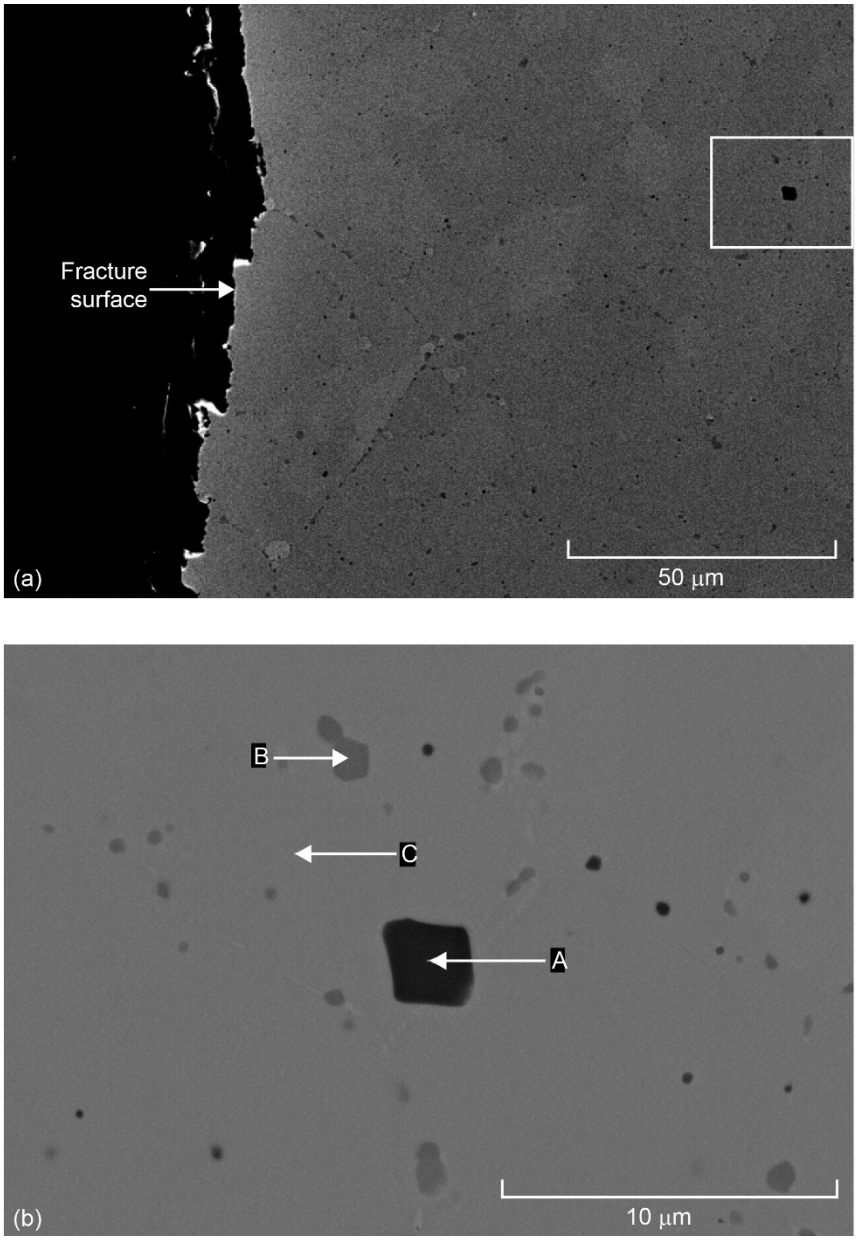

Figure 8.—SEM micrographs at (a) low and (b) high magnification of the bulk material perpendicular to the fracture surface shown in Figure 4 to Figure 7, showing a small (~2 μm), angular inclusion at *A*.

A section was made perpendicular to the fracture surface, approximately 1 mm away from the inclusion. This was done because metallographic preparation removes about a millimeter of material during grinding and polishing. The goal was to examine the material as close as possible to the fracture initiation site. SEM micrographs of the resulting cross section are shown in Figure 8. Another chemical inhomogeneity was observed approximately 100 μm from the fracture surface. Based on EDS analysis, as shown in Figure 9, the inclusion was composed of Ti and C and was, therefore, likely TiC. The same specimen used for this cross section was polished approximately 1 mm further into the bulk of the material. This cross section was then also examined by SEM and another angular inclusion was detected, as shown in Figure 10 and Figure 11. Hard, angular inclusions such as these would clearly serve as stress-risers within the bulk material enabling fracture initiation.

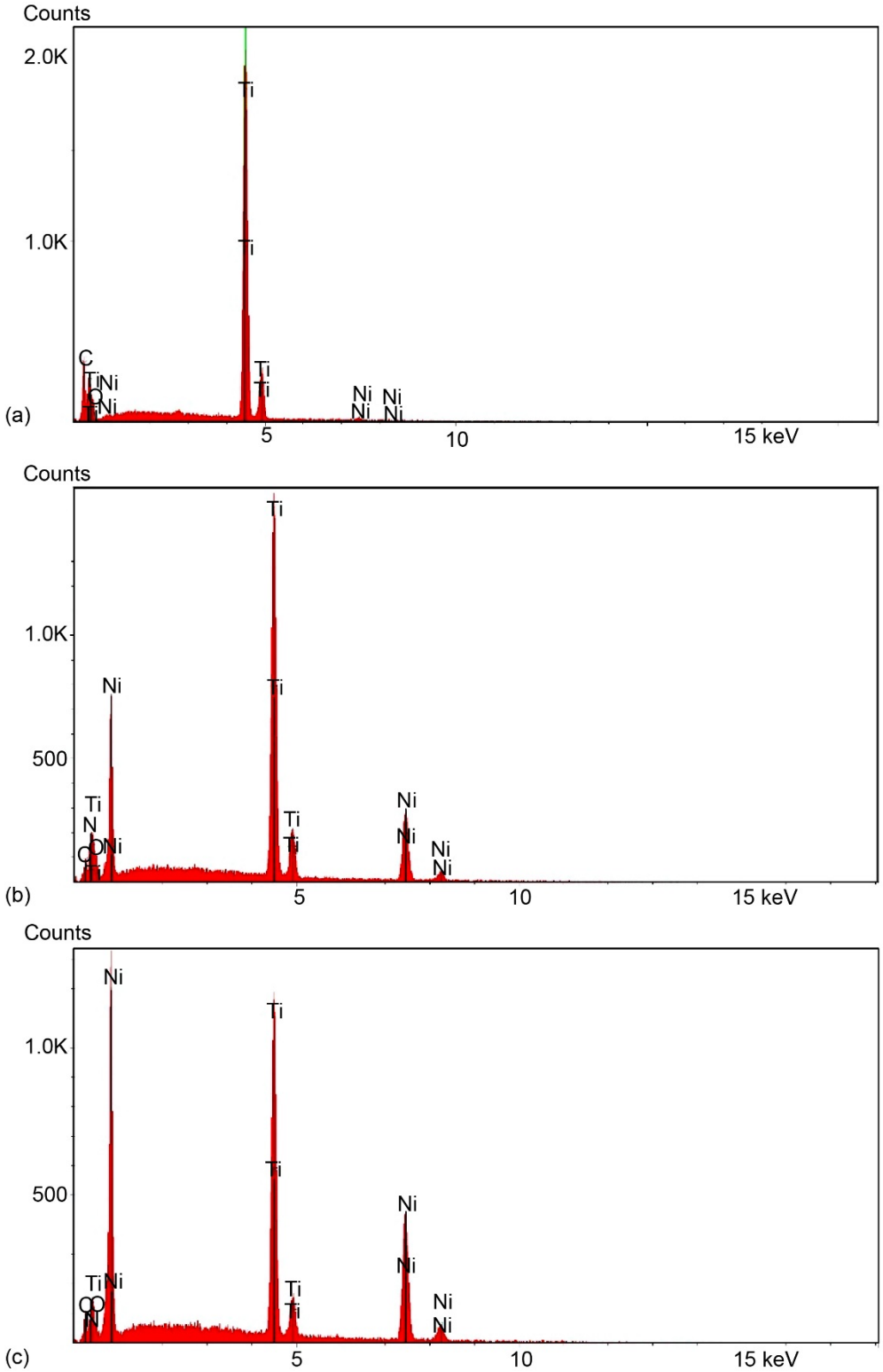

Figure 9.—Chemical analysis of the inclusion noted in Figure 8. The elements present (a) at point *A* are Ti, C, O and Ni, (b) at point *B* are Ti, Ni, C, O and N and (c) at point *C* are Ni, Ti, C and O.

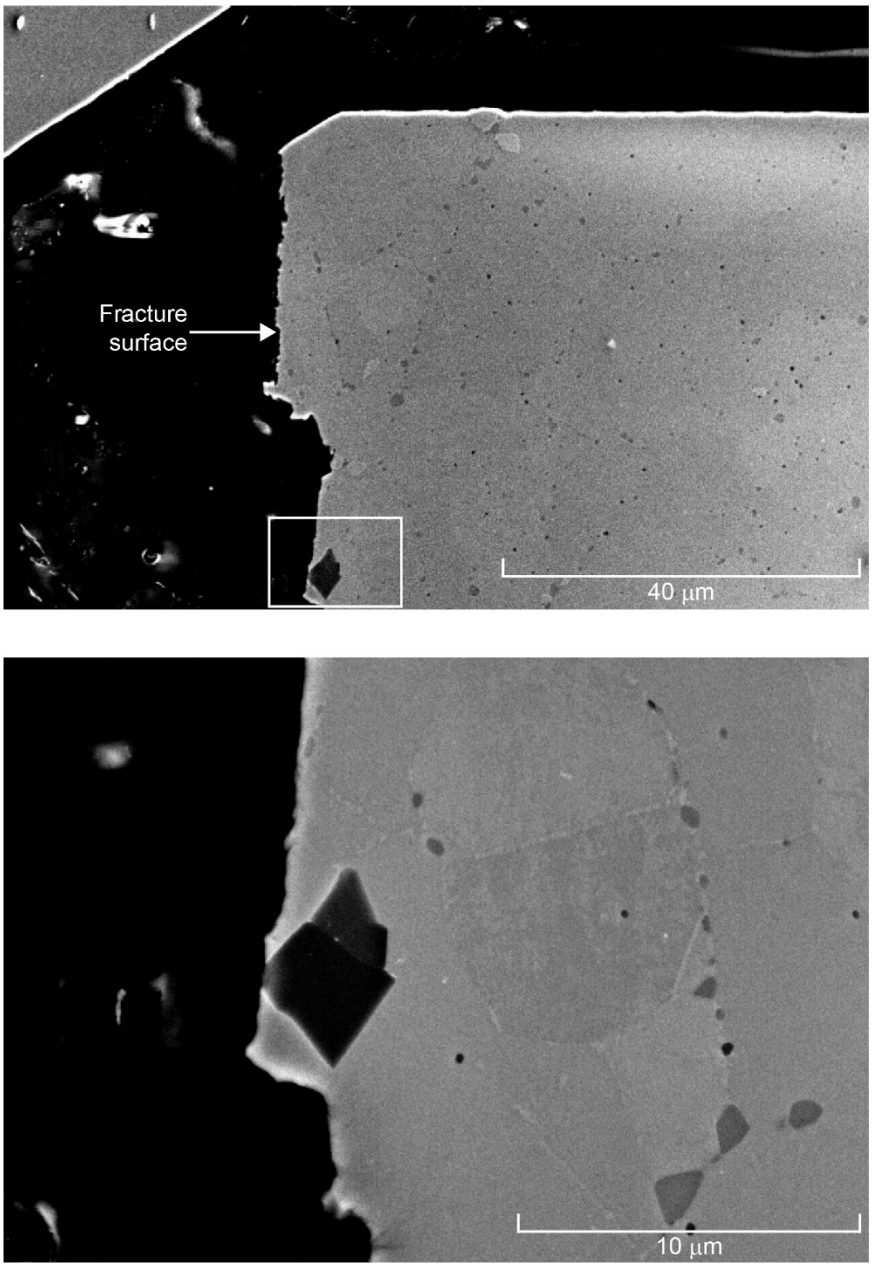

Figure 10.—SEM micrographs at (a) low and (b) high magnification of the bulk material perpendicular to the fracture surface shown in Figure 3 to Figure 6 and parallel to the surface shown in Figure 8 after additional polishing, showing another small (3 to 5 μm), angular inclusion.

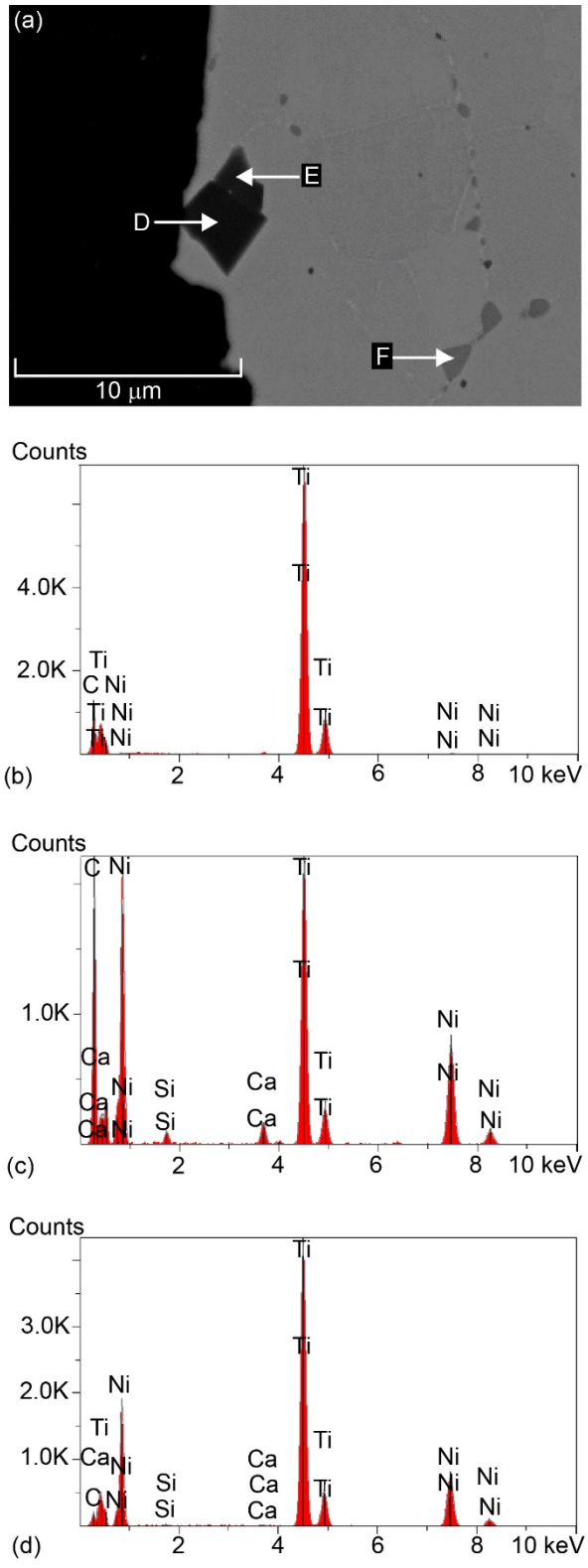

Figure 11.—Chemical analysis of the inclusion noted in Figure 10 (shown in a), indicating a composition of Ti and C. The spectra shown are for (b) location *D*, (c) location *E*, and (d) location *F*.

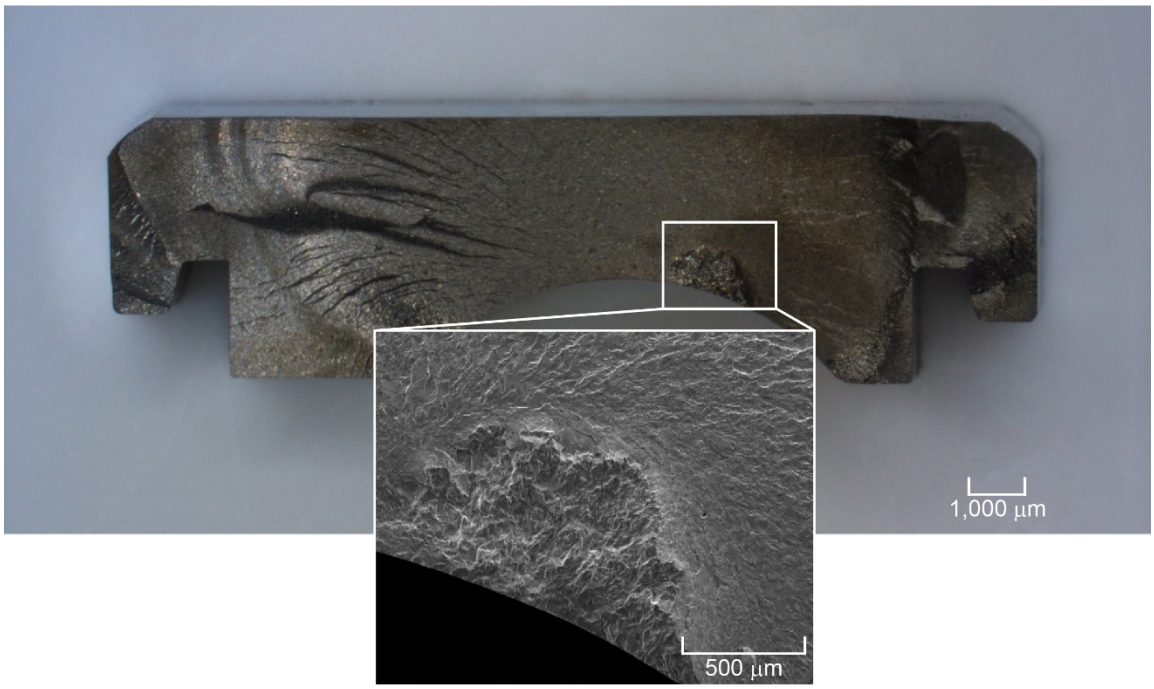

Figure 12.—Macroscopic image of a segment of the fractured bearing surface with the inset showing higher-magnification SEM image of the fracture origin.

A second fracture surface (from the fracture labeled “Fracture 2” in Figure 1) is shown in Figure 12. The fracture initiation site and the flaw within it are identified in Figure 13. Analysis of the flaw, shown in Figure 14, revealed that it was filled with particles with high concentrations of Ti, C and N, as with the inclusion that was previously discussed.

The location of these fracture origins may also be noteworthy. The fractures originated from the inner diameter of the outer bearing race, approximately 30° from top dead center. The mechanics of the state of stress at the fracture origins during bearing operation are beyond the scope of this investigation but may have an important role in these fractures.

A section of the bearing more than a centimeter away from any fractures was also selected for examination. This cross section was polished for metallographic examination. A macroscopic image of this cross section is shown in Figure 15. Inspection by optical microscopy revealed clusters of inclusions that had a golden appearance under the optical microscope in contrast to the typical bright white hue of the metallic Nitinol. Since pure TiN is known to have a golden hue and pure TiC is black, the visual appearance is further evidence that the inclusions are not pure TiC. They are likely TiCN or possibly TiN. EDS analyses of the inclusions, shown in Figure 16 and Figure 17, indicated that the composition of the inclusions were TiC, though the presence of N could not be excluded due to the peak interference between Ti and N mentioned previously. Regardless of the exact composition of the inclusion, it is a contaminant that is unexpected due to the cleanliness of the starting materials. Also, although this contamination appears to be present throughout the material, its presence coincides with both of the studied fracture initiation sites in this material. So, while contamination appears to play a critical role in these fractures, the presence of the contamination alone was not sufficient to cause fractures in the studied bearing. It is likely that the location (and, possibly, the concentration) of the contamination has the greatest effect on the initiation of the studied fractures since clusters of inclusions were found on the inner diameter of the bearing race at the fracture origins. The influence of the machining operation mentioned previously along with the likely combination of residual stresses in the part caused by heat treatment also cannot be ruled out as a possible additional factor in the initiation of the studied fractures.

Some context should be added to this discussion. Microscopic inclusions, like those discussed in this study, are found in many materials. So, the critical issue is not usually whether there are inclusions, but determination of the minimum size of an inclusion that will cause failure of the designed component and whether an inclusion of that size can be detected. In the bearing steel industry, methods have been developed to classify and detect inclusions down to a critical size (Refs. 10 to 15). From the fractures observed in this study, a concentration of inclusions within a certain volume (creating a larger *effective flaw size*), appears to be necessary to initiate a fracture in the given service environment. Since this study began, improvements have been made to the production methods for Nitinol such that large effective flaw sizes like the ones shown in this report (~100 μm) are no longer an issue. However, further work will be needed to classify and detect flaws of sizes critical to future applications.

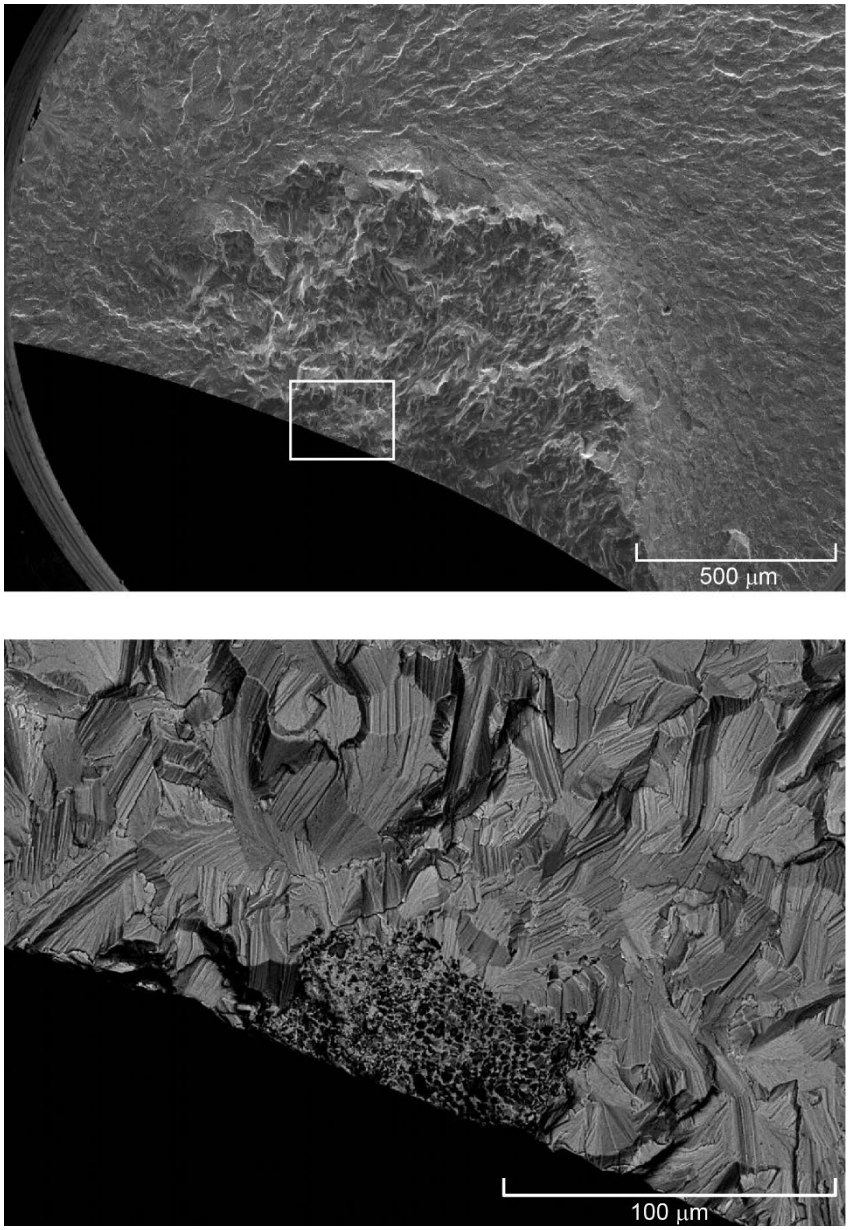

Figure 13.—SEM micrographs of the fracture initiation site shown in Figure 12 at (a) low and (b) high magnification, showing a cluster of inclusions (~100 μm in size).

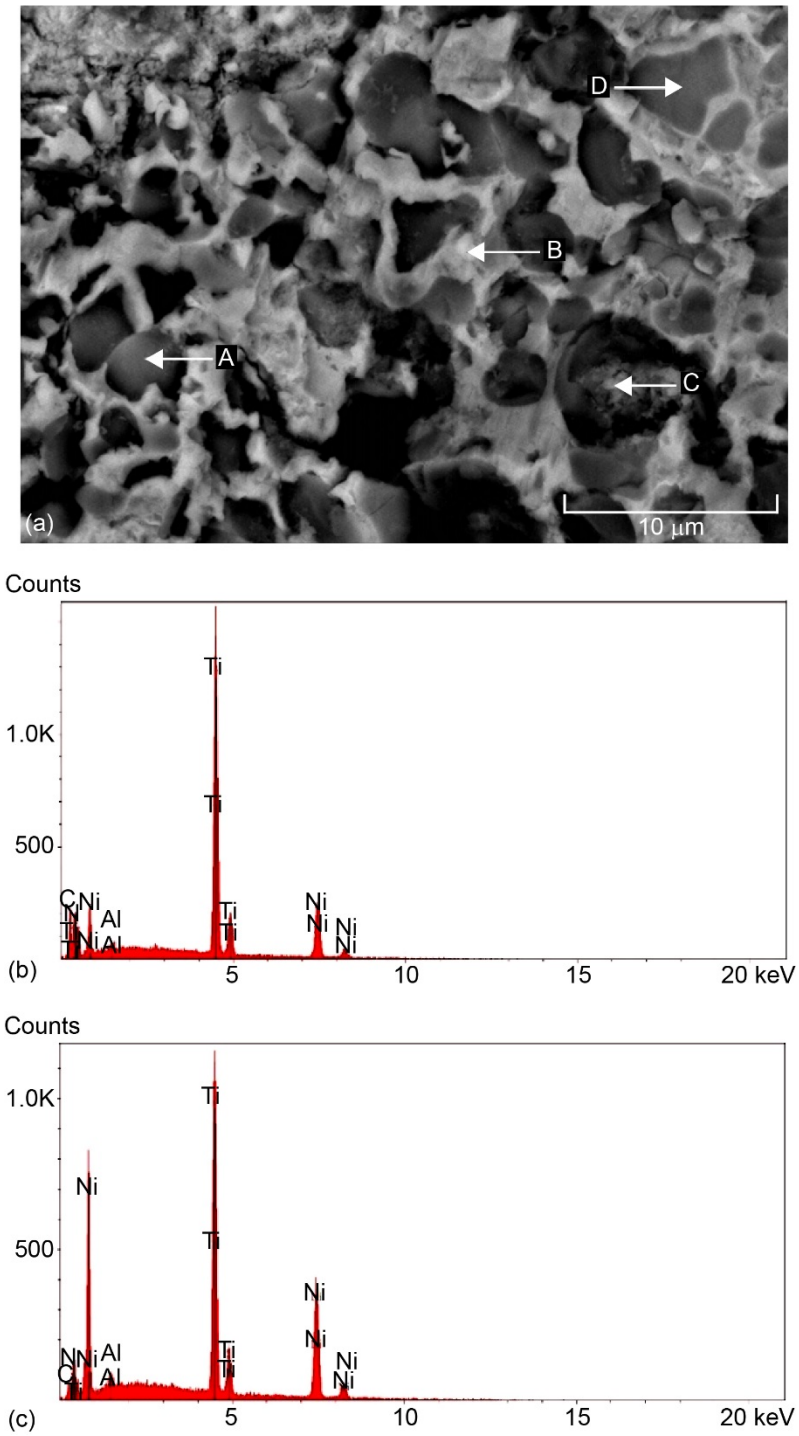

Figure 14.—(a) SEM of inclusions at fracture origin shown in Figure 13 with EDS chemical analyses indicating the presence of Ti-C-N based inclusions at (b) location *A*, (c) location *B*, (d) location *C* and (e) location *D*.

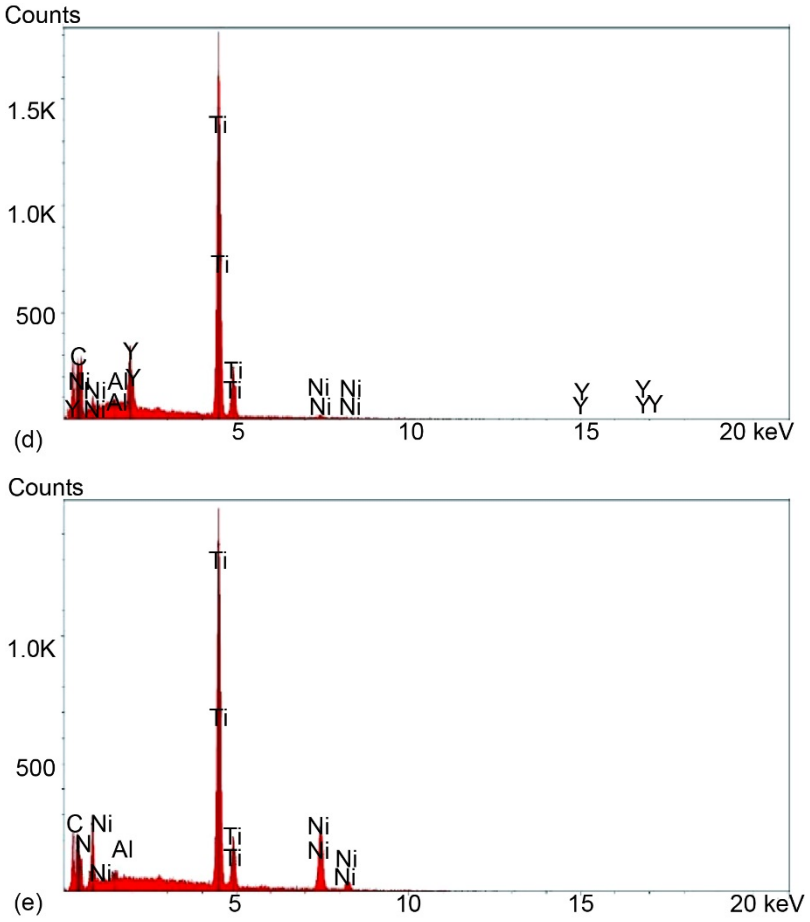

Figure 14.—Concluded.

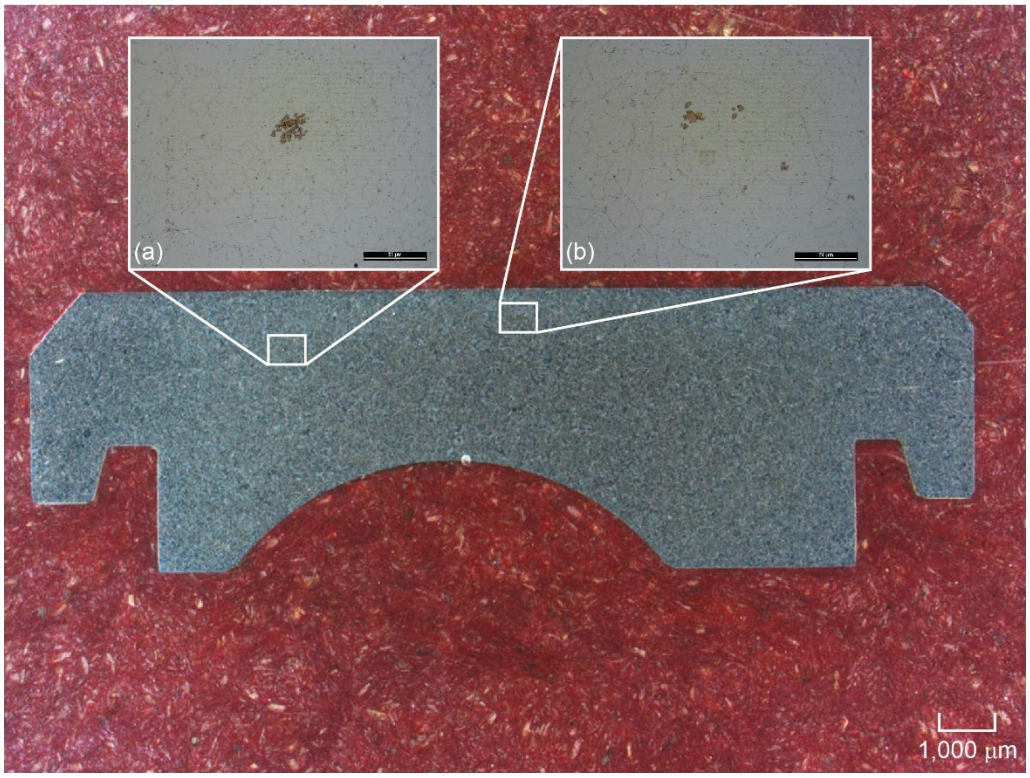

Figure 15.—Macroscopic image of random cross-section through the other race with insets (a) and (b) showing higher-magnification images of areas with additional inclusions, which have a golden hue under the optical microscope.

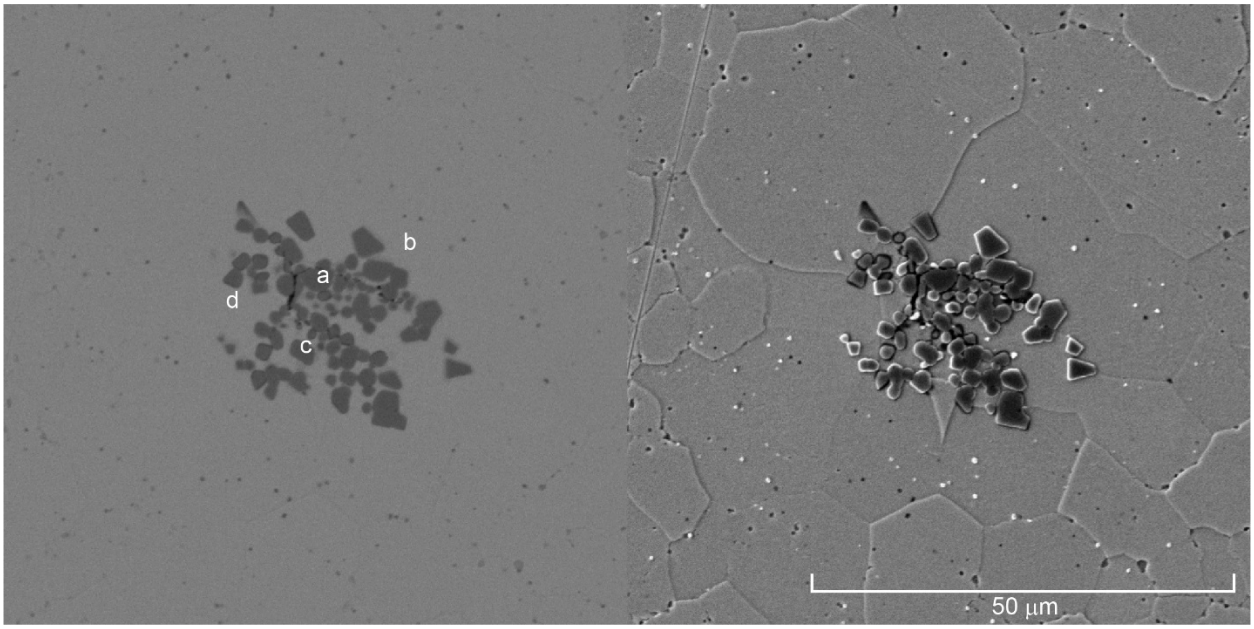

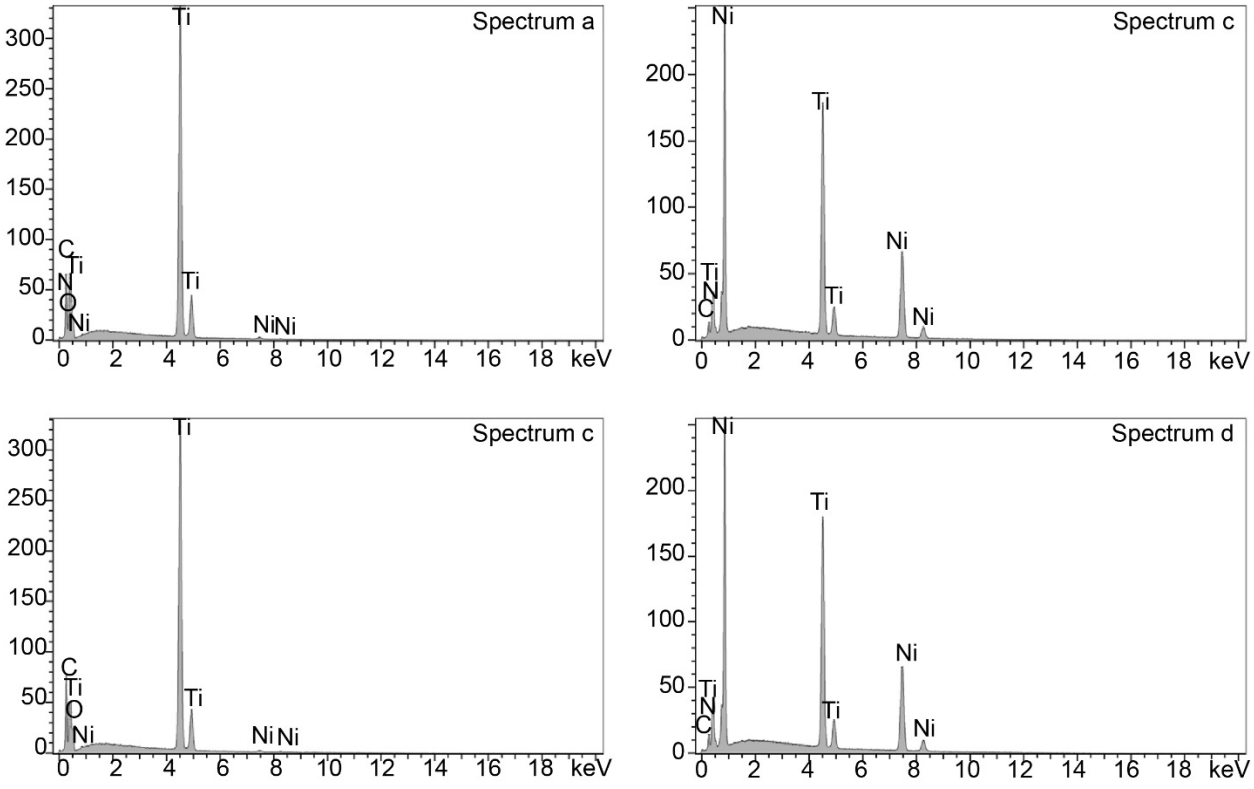

Figure 16.—Scanning electron micrographs and corresponding EDS spectra of inclusions shown in Figure 15(a) (the careful reader may notice that the optical image is inverted across the vertical axis compared to the SEM image). The image on the left is the backscattered electron image, which emphasizes atomic number contrast, and the image on the right is the secondary electron image, which emphasizes surface topography. Spectra correspond to the chemical compositions at locations labeled on the backscattered electron image.

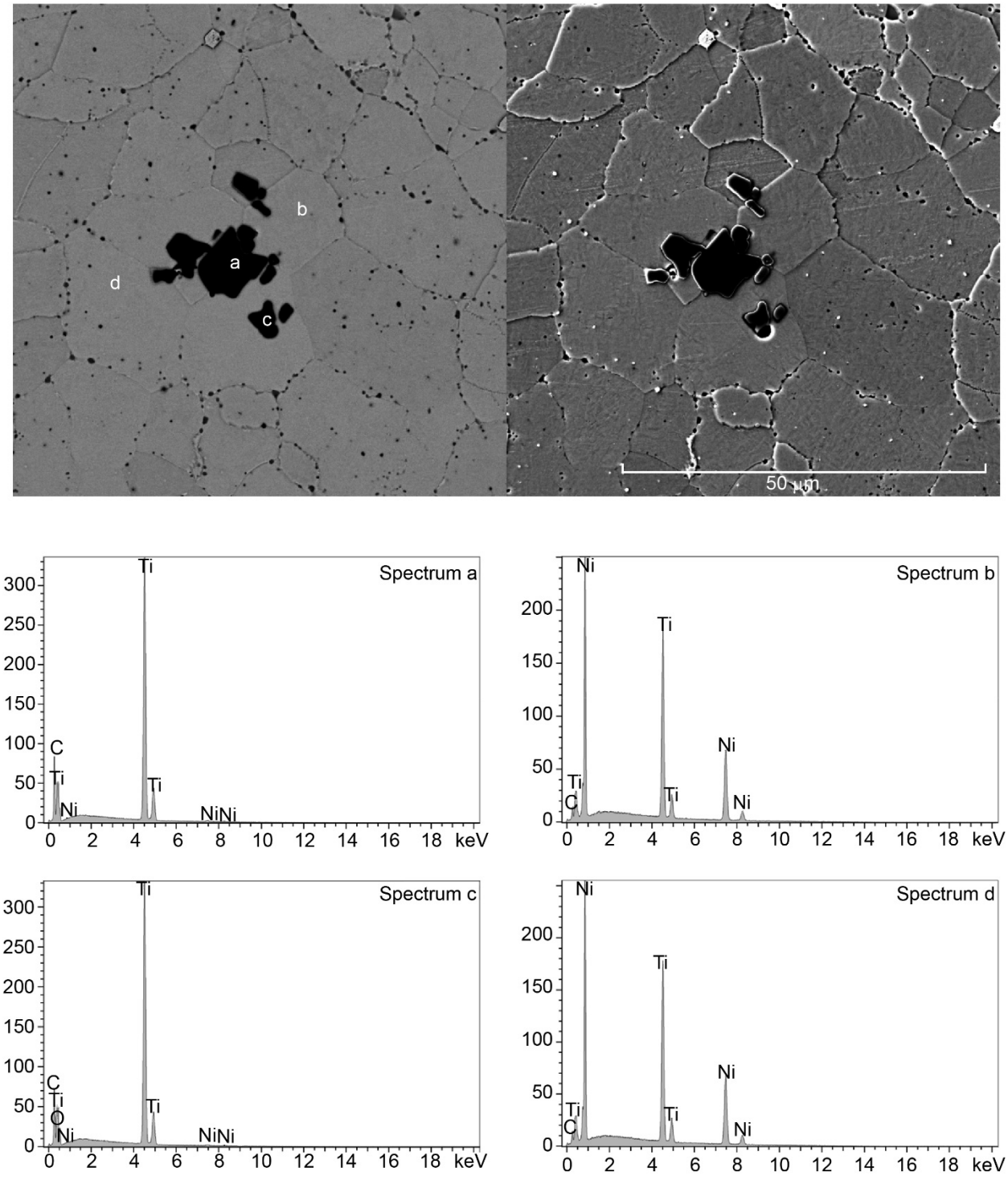

Figure 17.—Scanning electron micrographs and EDS spectra of inclusions shown in Figure 15(b) (the careful reader may notice that the optical image is inverted across the vertical axis compared to the SEM image). The image on the left is the backscattered electron image and the image on the right is the secondary electron image.

X-Ray Diffraction

The x-ray diffraction spectra showed multiple peaks representing separate phases that could not be isolated for identification. With the available instrumentation, isolated peaks are required at angles in the range of approximately 2θ = 120° to 150° for accurate classification (Ref. 17). However, as illustrated in Figure 18, multiple peak markers appear in the lower angle region from approximately 2θ = 45° to 115°. Therefore, the phases could not be identified and their lattice parameters could not be determined.

Specimens for x-ray diffraction generally require little preparation (Ref. 17). However, it was recently discovered that, for complex crystal structures like those found in intermetallic materials, a metallographic polish (one produced with mechanical polishing equipment resulting in a mirror finish) provided more precise results than those from a hand-polished sample (Ref. 18). It is possible that a polished surface on the bearing blanks could produce better results. However, polishing the surface also removes material that is under residual stress, which changes the state of stress the sample is under. Perhaps equipment and techniques will develop so that direct measurement will be possible with this material in the near future.

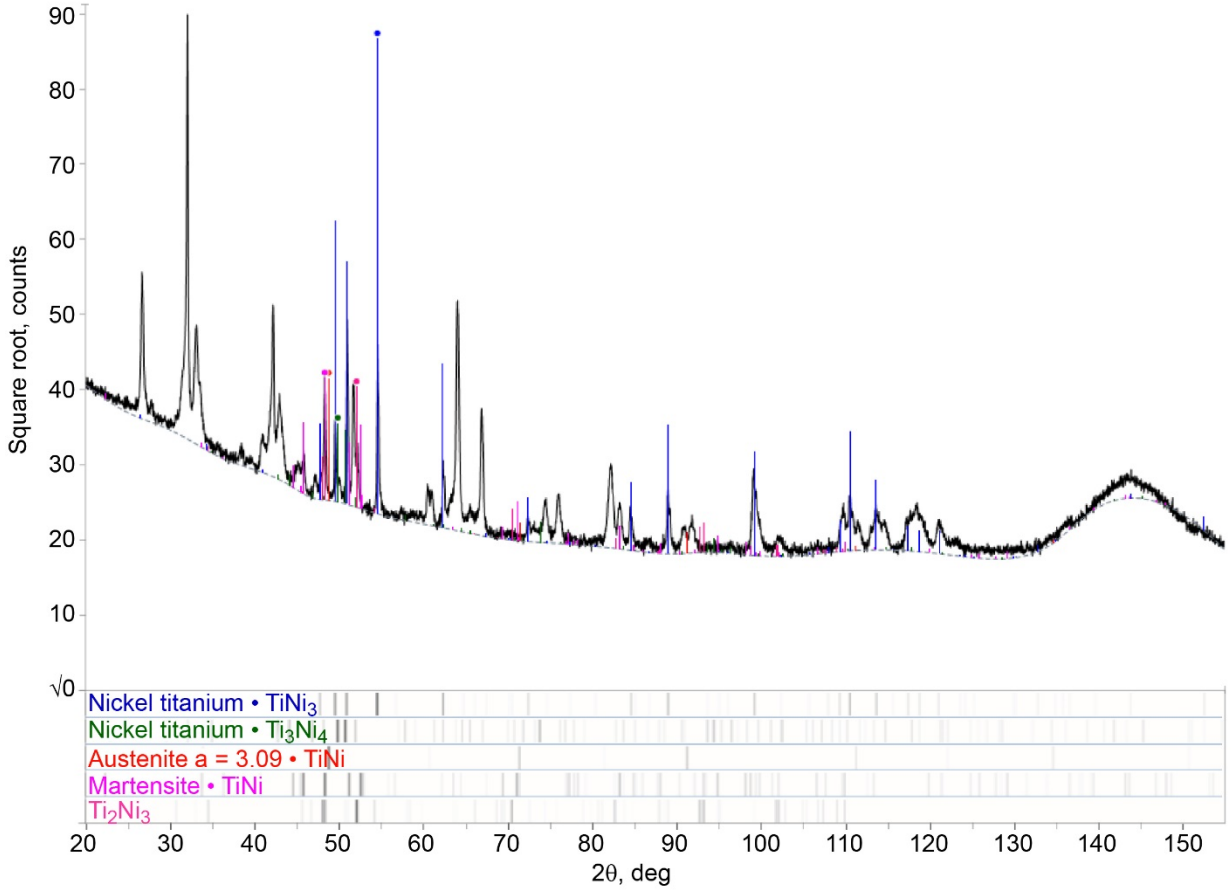

Figure 18.—X-ray diffraction spectrum (with phase identification near 2θ axis) for a 60-Nitinol bearing blank.

Conclusions

The fracture of a 60-Nitinol bearing was studied to determine the causes of the fracture. Based on the results of this study, the following conclusions have been made:

1. Fractures initiated at some of the larger clusters of TiC-based ceramic inclusions discovered in the material used to manufacture prototype components.
2. Other factors may have played secondary roles in the bearing failure including warping of the part due to excessive localized heating during machining. The warped part may have then experienced unbalanced loading during testing.
3. Residual stresses could not be measured using the available x-ray diffraction technique, primarily because the effect of residual stress on the individual phases is obscured by the range of possible phases detected within the material. As x-ray diffraction capabilities evolve and more phase identities are classified, this technique may be viable in the future.

References

1. C. DellaCorte, S.V. Pepper, R. Noebe, D.R. Hull, and G. Glennon, "Intermetallic Nickel-Titanium Alloys for Oil-Lubricated Bearing Applications," NASA/TM—2009-215646, March 2009, National Technical Information Service, Alexandria, VA.
2. S.V. Pepper, C. DellaCorte, R. Noebe, D.R. Hull, and G. Glennon, "NITINOL 60 as a Material for Spacecraft Triboelements," presented at the ESMATS 13 Conference, Vienna, Austria, September 2009.
3. C. DellaCorte, R. Noebe, M.K. Stanford, and S.A. Padula, "Resilient and Corrosion-Proof Rolling Element Bearings Made from Superelastic Ni-Ti Alloys for Aerospace Mechanism Applications," NASA/TM—2011-217105, National Technical Information Service, Alexandria, VA, September 2011.
4. C.D. Napoleon, private communication, 2012.
5. M.K. Stanford, "Hardness and Microstructure of Binary and Ternary Nitinol Compounds," NASA/TM—2016-218946, January 2016, National Technical Information Service, Alexandria, VA.
6. D.W. Richerson, "Modern Ceramic Engineering: Properties, Processing, and Use in Design," 2nd ed., Marcel Dekker, New York, 1992.
7. D.R. Askeland and Pradeep P. Phulé, "The Science and Engineering of Materials," 5th ed., Nelson Div. of Thompson Cananda, Toronto, 2006.
8. R.R. Adharapurapu, F. Jiang, and K.S. Vecchio, "Aging effects on hardness and dynamic compressive behavior of Ti-55Ni (at.%) alloy," Materials Science & Engineering A, vol. 527, pp. 1665–76, 2010.
9. M. Paryab, A. Nasr, O. Bayat, V. Abouei, and A. Eshraghi, "Effect of Heat Treatment on the Microstructural and Superelastic Behavior of NiTi Alloy with 58.5wt%Ni, Metalurgija – Journal of Metallurgy, vol. 16, no. 2, 2010, pp. 123–31.
10. M.K. Stanford, "Hot Isostatic Pressing of 60-Nitinol," NASA/TM—2015-218884, October 2015, National Technical Information Service, Alexandria, VA.
11. E.B. Pretorius, H.G. Oltmann, and B.T. Schart, "An Overview of Steel Cleanliness for an Industry Perspective," In AISTech Proceedings, pp. 6–9, 2013.
12. E. Fuchs and P. Jönsson, "Inclusion Characteristics in Bearing Steel Before and During Ingot Casting," High Temperature Materials and Processes, vol. 19, no. 5, pp. 333–343, May 2000.

13. S. Beretta and Y. Murakami, “Largest-Extreme-Value Distribution Analysis of Multiple Inclusion Types in Determining Steel Cleanliness,” Metallurgical and Materials Transactions B, vol. 32B, pp. 517–523, June 2001.
14. G. Shi, H.V. Atkinson, C.M. Sellars, C.W. Anderson, and J.R. Yates, “Statistical Prediction of the Maximum Inclusion Size in Bearing Steels,” Bearing Steel Technology, ASTM STP 1419, J.M. Beswick, ed., American Society for Testing and Materials International, West Conshohocken, PA, 2002.
15. T. Nishikawa, H. Nagayama, S. Nishimon, K. Asai, I. Fujii, and T. Sugimoto, “Study of Evaluation Method for Non-Metallic Inclusions and Development of Slag Refining for Bearing Steel,” Bearing Steel Technology, ASTM STP 1419, J.M. Beswick, ed., American Society for Testing and Materials International, West Conshohocken, PA, 2002.
16. Y. Kato, K. Sato, K. Hiraoka, and Y. Nuri, “Recent Evaluation Procedures of Nonmetallic Inclusions in Bearing Steels (Statistics of Extreme Value Method and Development of Higher Frequency Ultrasonic Testing Method),” Bearing Steel Technology, STP 1419, J. M. Beswick, ed., American Society for Testing and Materials International, West Conshohocken, PA, 2002.
17. P.S. Prevey, “X-Ray Diffraction Residual Stress Techniques,” in ASM Handbook, vol. 10: Materials Characterization, ASM International, Materials Park, OH, 1986, pp. 380–92.
18. R.B. Rogers, unpublished report.